ELSEVIER

Journal of Nuclear Materials 241–243 (1997) 385–340

journal of nuclear materials

# Erosion/redeposition at the JET MkI divertor

H.Y. Guo [a,*], J.P. Coad [a], S.J. Davies [a], J.D. Elder [a,b], L.D. Horton [a], X.L. Li [a], J. Lingertat [a], A. Loarte [a], G.F. Matthews [a], R.D. Monk [a], R. Simonini [a], M.F. Stamp [a], P.C. Stangeby [a,b], A. Tabasso [a,c]

[a] *JET Joint Undertaking, Abingdon, Oxfordshire OX14 3EA, UK*
[b] *University of Toronto, Institute for Aerospace Studies, Toronto, Canada*
[c] *Imperial College, Plasma Physics Department, Blackett Laboratory, London SW7 2BZ, UK*

**Abstract**

The DIVIMP/NIMBUS codes are employed to simulate divertor carbon profiles and the net erosion measured by colorimetry using the most recent chemical sputtering data and models. The relative roles of physical and chemical sputtering are assessed in terms of erosion and impurity contamination. Beryllium photon fluxes are also modelled, showing much less sputtering than predicted by the pure beryllium sputtering data. In addition, the erosion of fixed divertor target Langmuir probe tips has been measured photographically and gives an effective sputtering yield of $< 0.5\%$.

*Keywords:* JET; Impurity source; Chemical erosion; Erosion and particle deposition; Monte Carlo simulation

## 1. Introduction

Erosion/redeposition is one of the crucial physical issues to be faced in the design of a fusion reactor such as ITER. The erosion of plasma facing components (PFCs) limits the life time of a reactor and also produces impurity influxes which degrade fusion performance. In addition, the redeposition of the PFCs is a major concern regarding the tritium in-vessel inventory. For most materials, the dominant erosion process is physical sputtering whilst for graphite, chemical sputtering has also proven to be important [1]. However, it is unclear what the consequences of this are for erosion and plasma contamination since not only does chemical sputtering exhibit an uncertain flux dependence but also there is the possibility of prompt local redeposition of molecular ion fragments [2–4]. Spectroscopic measurements at TEXTOR [5] show a strong reduction of $CD_4$ formation under high flux deuteron bombardment, $\sim \Gamma^{-0.5}$, while the multi-machine data base compiled by Vietzke and Haasz [6] has a weaker flux dependence $\sim \Gamma^{-0.1}$ ($\Gamma$ is the bombarding flux density). However, they both give a yield of $\sim 1\%$ for the ion flux of about $5 \times 10^{23}$ $D^+$ $m^{-2}$ $s^{-1}$, which is typical of divertor conditions. In addition, the recent data obtained by Haasz et al. [7] at low flux ($3 \times 10^{18}$ $D^+$ $m^{-2}$ $s^{-1}$) show a strong energy dependence for $CD_4$ production with a yield of $< 1\%$ at an ion impact energy of 10 eV. Roth and Garcia-Rosales' newly revised formula [8], which is based on the measurement of the methane yield, also shows such reduction of the chemical sputtering yield at low energy and includes stronger flux dependence compared to their previous formula [9]. It is to be noted that the measurements of the chemical sputtering yield are subject to large uncertainties, especially the spectroscopic data, due to simultaneous bombardment of ions and neutrals and uncertainties in atomic data for hydrocarbon break-up (for the determination of $CD_4$ yield from the C–D band) and $D_\alpha$ measurements. In addition, higher hydrocarbons such as $C_2D_x$ may also contribute significantly to the chemical sputtering, especially at low ion energies [10].

Beryllium has been chosen as the baseline material for ITER. One serious concern is the life time of the beryllium PFCs which may suffer from severe plasma sputtering

* Corresponding author. Tel.: +44-1235 464 970; fax: +44-1235 464 766; e-mail: hguo@jet.uk.


*PII* S0022-3115(96)00534-X

based on the pure beryllium data base for sputtering [11]. The recent finding by Hirooka et al. [12] demonstrates a much smaller sputtering yield for beryllium in the presence of trace carbon which can form thin carbon films on the beryllium surface and protect beryllium from erosion. At the end of the JET MkI campaign, the graphite divertor tiles were replaced by beryllium tiles. The information on the erosion of the beryllium targets is particularly useful to confirm this important finding.

In this article we report the direct measurement of erosion rates at the JET divertor target plate using colorimetry and the behaviour of impurity fluxes in the graphite and beryllium divertor under various operational regimes, as well as detailed modelling using the DIVIMP/NIMBUS codes [13,14] for the validation of the most recent chemical sputtering data base and the models. Sputtering at the beryllium target is also investigated.

## 2. Experiment and modelling

During the 1994–1995 JET operation a colour viewing system has been used to measure erosion/redeposition from changes in the complementary colours of redeposited films [15] using the method of Wienhold et al. [16]. A CCD colour video camera views the outer part (400 × 350 mm) of the divertor floor from the top of the vessel using illumination provided by a halogen lamp with a dichroic reflector. Colour images are taken automatically after each pulse using a frame grabber. With an analysis program, the colour coordinates RGB (red, green, blue) of images are converted to hue values, which are then related to the film thickness. Divertor carbon (C(II))/beryllium (Be(II)) intensity profiles have been recorded with an absolutely calibrated flux camera, which views the divertor vertically from the top of the vessel. In addition, visible spectroscopy has been employed to measure the integrated photon flux of C(III)/Be(II) from the inner and outer divertor areas separately.

For the investigation of impurity production and erosion at the divertor target plates, the DIVIMP code, coupled to the 2D NIMBUS Monte-Carlo neutral code, is employed to simulate measured erosion and carbon/beryllium profiles under various operational regimes. A 2D background plasma is generated using 'onion-skin' models, based on the measurements of Langmuir probes at the target plates to define boundary conditions [17,18]. In addition, the 2D solutions of the 2D edge fluid code EDGE2D [19] can also be directly coupled to DIVIMP as background plasma. Then, impurity neutrals are launched using both physical and chemical sputtering resulting from the impact of ions (on the target) and atoms (on all the vessel surfaces). The sputtered particles are assumed to be emitted with a cosine angular distribution and different velocity distributions: a Thompson velocity distribution for physically sputtered atoms; the chemically sputtered atoms have a given energy corresponding to the wall temperature (the actual $CD_4$ break-up processes are not yet modelled by DIVIMP). Particles are followed through each ionisation state until they redeposit on the target plates or on the wall.

In particular, the following options for chemical sputtering have been recently implemented in the DIVIMP/NIMBUS code based on: (1) TEXTOR data [5], (2) Vietzke and Hassz's compiled data base (V-H) [6], (3) new data from Toronto [7], and (4) Roth and Garcia-Rosales' revised formula (R-G '96) [8].

## 3. Results and discussions

### 3.1. Impurity behaviour in the CFC / Be divertor

JET MkI campaign experienced both the CFC and beryllium divertor target operations. Detailed assessment of plasma performance of these targets are described by Campbell [20]. In particular, different sputtering characteristics of carbon and beryllium can be clearly seen in Figs. 1 and 2, which show the evolution of impurity fluxes, together with a Langmuir probe ion saturation current, $J_s$, with increasing plasma line averaged density, for two ohmic density limit discharges for CFC and beryllium targets, respectively. As can be seen in Fig. 1, as plasma density increases, ion particle fluxes to the inner and outer CFC target plates initially increase, then decrease, showing plasma detachment at the targets. It is to be noted that for this discharge the strike zones move across the target at a frequency of 4 Hz, the peaks in the $J_s$ correspond to the maximum value at the strike point. The envelope gives the

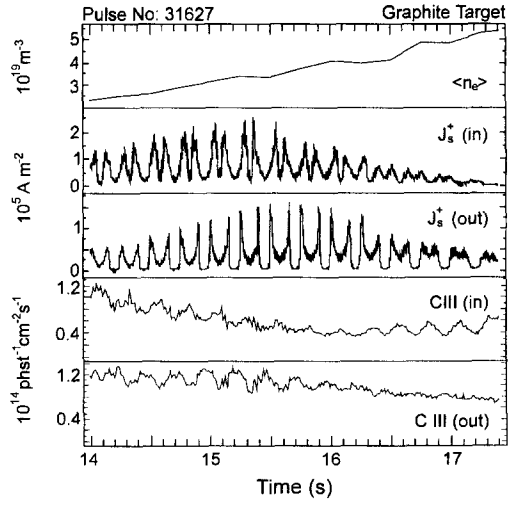


Fig. 1. Evolution of plasma line averaged density, ion saturation current to the inner, outer divertor target plates and C(III) photon fluxes (integrated over both targets) for the ohmic density limit discharge 31627.

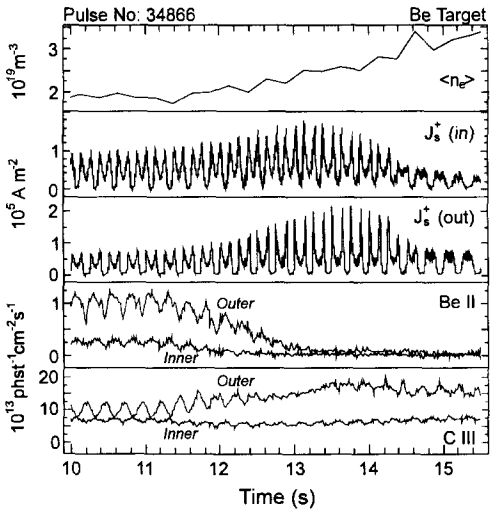


Fig. 2. Behaviour of divertor Be(II) and C(III) photon fluxes for the ohmic density ramp discharge (34866) at the beryllium targets.

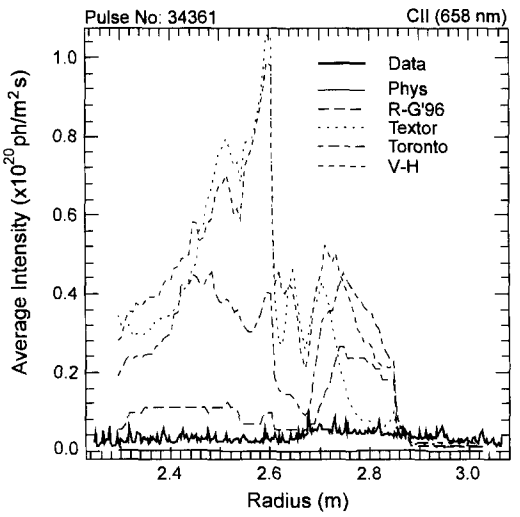


Fig. 4. Divertor C(II) profile and code predictions for shot 34361 at divertor detachment.

time evolution of the peak ion saturation current. C(III) photon fluxes initially fall then saturate, suggesting that chemical sputtering becomes dominant. As for the beryllium case (Fig. 2), the plasma density and ion fluxes to the divertor plates evolve similarly to the CFC target. However, as the plasma starts to detach from the target, the electron temperature measured by the Langmuir probes at the target plates decreases down to a value below 5 eV, Be(II) emission, as shown in Fig. 2, decreases to very low levels, as expected from purely physical sputtering. In addition, the average C(III) intensity in the outer divertor shows a tendency to increase as the plasma line averaged density increases, indicating the presence of chemical sputtering from the main chamber (into the sight line of the spectrometer).

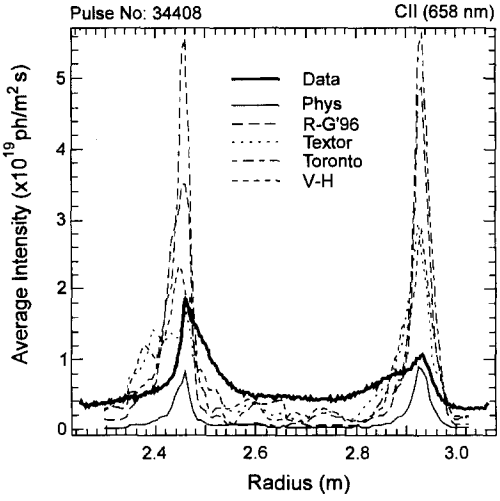


Fig. 3. C(II) photon fluxes along the divertor target for the low density ohmic discharge 34408, together with calculated results from the DIVIMP code using the most recent chemical sputtering data and models.

### 3.2. Divertor carbon profiles

In an attempt to better understand the impurity production mechanisms and to validate the current chemical sputtering data and models, we have carried out more detailed simulations of the divertor carbon profiles measured under different operational regimes using the DIVIMP/NIMBUS codes. Fig. 3 shows the C(II) photon flux poloidal distribution along the divertor target for a low density ohmic discharge (34408), together with the code predictions.

For this case, the electron temperature and density at the strike points as measured by the target Langmuir probes are: $T_e = 20.7$ eV, $n_e = 3.9 \times 10^{18}$ m$^{-3}$ at the outer strike point, and $T_e = 13.8$ eV, $n_e = 6.9 \times 10^{18}$ m$^{-3}$ at the inner strike point. The background plasma is generated using the target Langmuir probe data as input to an 'onion-skin' plasma model assuming $T_i = T_e$. The cross-field diffusion coefficient was taken to be $D_\perp = 1$ m$^2$/s for impurity ions. Chemically sputtered atoms are launched from the target (600 K) and the wall (300 K) with the yields from various data bases and models as indicated in Fig. 3. As can be seen at the strike zones, the Toronto data (at low flux) and also the other data using flux-dependant yields produce too high C(II), especially at the outer divertor. At the strike points, the experimental data can be reproduced by using physical sputtering +20% R-G '96 chemical sputtering, for example. At the private region, the C(II) line intensity is underestimated by all the chemical sputtering models due to inadequate neutral source ob-

tained by the NIMBUS code. In the simulations, the chemically sputtered carbon atoms are assumed to have a initial energy of 0.1 eV, but varying this energy from 0.05–0.5 eV causing little changes in the calculated C(II) profiles.

At divertor detachment, the electron temperature at the target plates is so low (< 1 eV) that chemical sputtering should dominate. Fig. 4 shows the measured C(II) profile and simulated results for such a case. Since it is difficult to measure electron temperature in this regime, the EDGE2D generated background plasma for this pulse [19] is used in DIVIMP. It is evident that the data with flux dependence still predicts too high C(II) intensity, compared with the experimental data. The formula of Roth and Garcia-Rosales (R-G '96) produces the lowest C(II), which is, however, still a factor of 5 higher than the measurements. This would indicate that apart from the flux dependence, the efficiency of the break-up of $CD_4$ to produce $C^+$ ions could be low. However, the observation could also be due to strong reduction of $CD_4$ production at low energy as indicated by the Toronto data.

### 3.3. Erosion at the graphite target

The erosion rates at the divertor targets, determined by colorimetry, are strongly dependent on the stability of the strike point position and the power deposition on the targets. For example, in a discharge with 10 MW of additional heating and moderate density an erosion rate of about 5 nm/s is observed near the strike point. Sweeping of the strike zones greatly reduces the erosion except at the turning points of the sweep, as would be expected [15]. At high power, much higher erosion rates have been observed. Fig. 5 shows the erosion/redeposition profiles for a hot ion H-mode discharge. For this pulse, the total heating power was initially 22 MW, then stepped down to 12 MW, with a duration of about 1 s in total. The strike point was very stable during this period. The plasma parameters at the target plates, as measured by Langmuir probes, also remained constant. As can be seen the profile is peaked and narrow (~ 1 cm) with a net erosion of about 20 nm near the strike point. Eroded atoms are redeposited nearby in the private region. The calculated net/gross erosion profiles are also shown in Fig. 5. The Langmuir probe measurements at the target are used as input to the DIVIMP code assuming $T_i = 6T_e$ ($T_e \sim 40$ eV, 30 eV at the inner/outer targets), yielding target plate power flux of 5 MW, which is in reasonable agreement with IR measurements (~ 6 MW in the ELM-free phase of a hot ion H-mode [21]). The chemical sputtering yield is calculated according to the revised formula by Roth and Garcia-Rosales. The cross-field diffusion coefficient is assumed to be $D_\perp = 0.2$ m$^2$/s. As can be seen the net erosion caused by physical sputtering alone results in a very peaked profile, in agreement both in magnitude and in shape with the experimental data. Including chemical sputtering, the gross erosion is increased significantly. However, the net erosion shows little change. It should be noted that the erosion/redeposition profile is very sensitive to the impurity transport. With $D_\perp = 1$ m$^2$/s, the peak net erosion produced by chemical sputtering increases to ~ 30 nm while the peak net erosion amounts to ~ 20 nm for physical sputtering. The net redeposition in the private region increases dramatically for these cases: 35 nm for physical sputtering alone and 65 nm including chemical sputtering.

Additional information on erosion/redeposition has come from the fixed target Langmuir probe tips that were

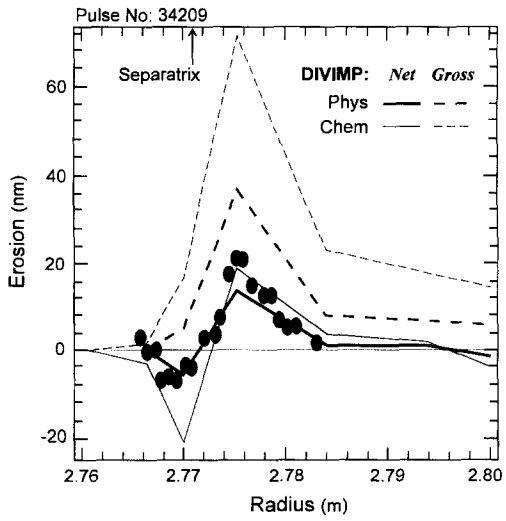


Fig. 5. Erosion profiles measured by colorimetry and calculated results for a hot ion H-mode: 34209.

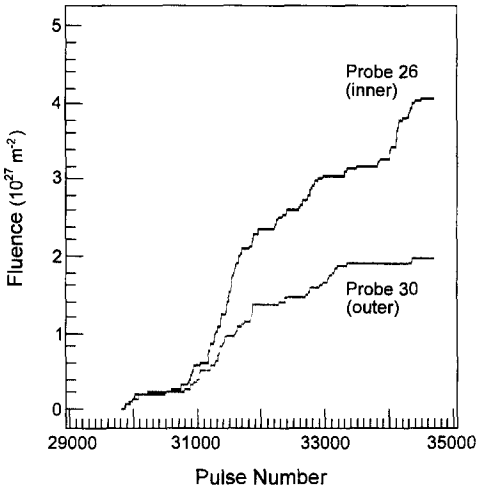


Fig. 6. Deuteron fluence exposed to the probe tips: #26 (at the inner target) and #30 (at the outer target), as a function of pulse number over the MkI campaign.

removed after the MkI CFC campaign. These tips were made of pyrolitic graphite and changes in surface profile were measured photographically, showing no obvious degradation of probe area. The only significant change in appearance was a slight rounding of the corners. Those tips from the high fluence region of the target showed erosion of ~0.1 mm–0.2 mm. Fig. 6 shows the deuteron fluence exposed to the probe tips at the high and low flux regions as a function of pulse number over the MkI campaign. This was obtained by integration of the ion saturation current from the triple probes which were available for most pulses over the whole discharge. The total fluence to the tip from the high fluence region amounted to $4 \times 10^{27}$ $m^{-2}$. This implies an effective sputtering yield of $< 0.5\%$.

### 3.4. Sputtering of the beryllium target

Detailed DIVIMP modelling has been performed for the discharge (34866) on the beryllium divertor target, using the sputtering yield for pure beryllium and beryllium oxide, for two phases: low recycling (10 s) and high recycling (14 s) phases, respectively. The global parameters of the discharge are shown in Fig. 2. At low recycling, $T_e$ is about 20 eV at both the inner and outer strike points with $n_e$ at $2.5 \times 10^{19}$ $m^{-3}$. At high recycling, $T_e$ at the outer divertor falls to about 10 eV, while the inner divertor is detaching. At this stage, the divertor probes tend to overestimate the electron temperature [22]. Therefore, the plasma background generated by EDGE2D is coupled to the DIVIMP code.

Fig. 7 shows the measured Be(II) profile and the results calculated by the DIVIMP code for the low recycling phase. It appears that using the pure Be sputtering yield results in an overestimate of the Be(II) photon fluxes,

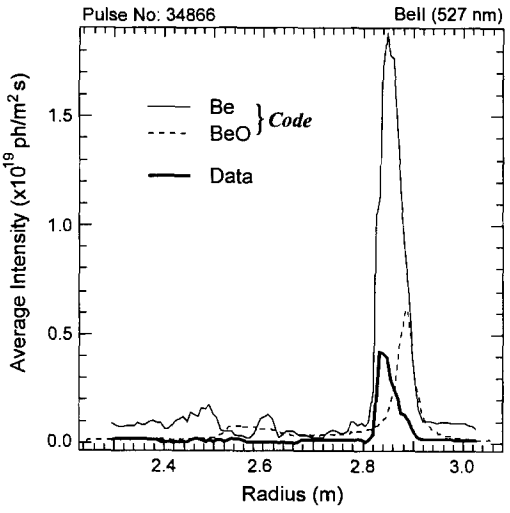


Fig. 7. Comparison of measured Be(II) photon fluxes and results calculated by the DIVIMP code using the sputtering data for Be and BeO for the low recycling phase for pulse 34866.

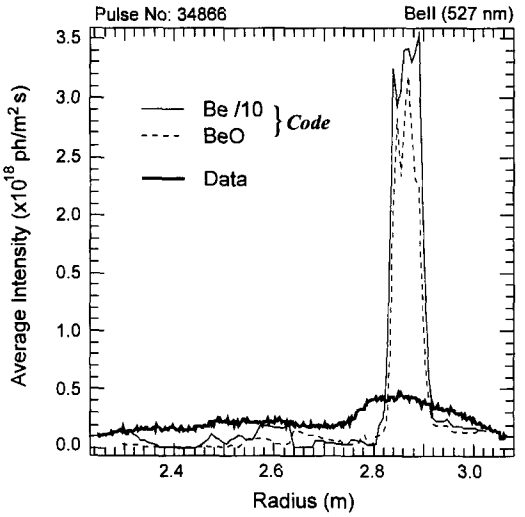


Fig. 8. Measured and simulated Be(II) photon fluxes for the high recycling phase of the discharge 34866.

while the BeO sputtering yield fits the data better. For the high recycling phase, as shown in Fig. 8, the Be intensity is significantly overestimated with the pure Be yield. Even the BeO yield also predicts too high Be(II). It is to be pointed out that the presence of the water cooled divertor modules kept the temperature of the divertor tiles at typically ~50°C between pulses. For pulse 34866, as the discharge evolved from the initial low recycling phase to the high recycling phase, the divertor target temperature, as measured by the IR camera, increased to ~460°C. It has been observed that above ~280°C beryllium and the surface oxide can inter-diffuse, thus resulting in a clean beryllium surface [23]. In addition, the presence of oxygen impurity in the plasma is unlikely to form surface oxides under high flux ($\sim 10^{23}$ $m^{-2}$ $s^{-1}$) deuteron bombardment. Therefore, the above result would appear to be best explained by the recent finding of Hirooka et al. that the sputtering of beryllium can be significantly reduced by carbon poisoning at high surface temperatures.

## 4. Conclusions

The simulation of the divertor carbon profiles shows that at the strike zone (high flux region), the chemical sputtering yield of $CD_4$ using a flux dependence factor still overestimates C(II) photon fluxes. This indicates low efficiency of producing $C^+$ ions from $CD_4$ (~20%). The net erosion measured by colorimetry is reproduced by the DIVIMP code with a dominant physical sputtering source, and shows that the gross erosion is reduced significantly due to redeposition. In addition, the erosion of target Langmuir probe tips implies an effective yield of $< 0.5\%$, also indicating an important contribution from redeposi-

tion. Beryllium targets show a much smaller sputtering yield than expected for pure beryllium sputtering yield, possibly due to beryllium oxidation and/or carbon contamination.

## References

[1] J. Roth, E. Vietzke and A.A. Haasz, Nucl. Fusion 1 (1991) 63, Suppl.
[2] G. Lieder, K. Behringer, A.R. Field et al., in: Proc. of 21st EPS Conf. on Controlled Fusion and Plasma Physics, Vol. 18B, Part II, Montpellier, 1994, p. 722.
[3] K. Shimizu et al., IAEA-CN-60/D-P-I-2, 15th IAEA Conf., Seville, Spain, 1994.
[4] A. Kallenbach, R. Neu, W. Poschenrieder et al., Nucl. Fusion 34 (1994) 1557.
[5] A. Pospieszczyk et al., these Proceedings, p. 833.
[6] E. Vietzke and A.A. Haasz, in: Physical Processes of the Interaction of Fusion Plasmas (Academic Press Inc., 1996) ch. 4, p. 135.
[7] A.A. Haasz, B.V. Mech and J.W. Davis, J. Nucl. Mater., submitted.
[8] J. Roth and C. Garcia-Rosales, Nucl. Fusion, submitted.
[9] C. Garcia-Rosales and J. Roth, in: Proc. of 21st EPS Conf. on Controlled Fusion and Plasma Physics, Vol. 18B, Part II, Montpellier, 1994, p. 770.
[10] J.W. Davis and A.A. Haasz, these Proceedings, p. 37.
[11] W. Eckstein, C. Garcia-Rosales, J. Roth and W. Ottenberger, Sputtering Data, IPP-Garching Rep. 9/82 (1993).
[12] Y. Hirooka et al., J. Nucl. Mater. 230 (1996) 173.
[13] P.C. Stangeby, C. Farrell, S. Hoskins and L. Wood, Nucl. Fusion 28 (1988) 1945.
[14] P.C. Stangeby and J.D. Elder, J. Nucl. Mater. 196–198 (1992) 258.
[15] H.Y. Guo et al., in: Proc. of 22nd EPS Conf. on Controlled Fusion and Plasma Physics, Vol. 19C, Part II, Bournemouth, 1995, p. 273.
[16] P. Wienhold, F. Weschenfelder and J. Winter, Nucl. Instrum. Methods Phys. Res. B 94 (1994) 503.
[17] P.C. Stangeby et al., these Proceedings, p. 358.
[18] S.K. Erents et al., these Proceedings, p. 433.
[19] A. Loarte et al., these Proceedings, p. 118.
[20] D.J. Campbell et al., these Proceedings, p. 379.
[21] G.K. McCormick et al., these Proceedings, p. 444.
[22] R.D. Monk et al., these Proceedings, p. 396.
[23] J. Roth, J. Nucl. Mater. 145–147 (1987) 87.